# Analysis of Oxide and Vanadate Supports for Catalytic Hydrogen Combustion: Kinetic and Mechanistic Investigations

**Parag A. Deshpande, Sneha Polisetti, and Giridhar Madras**
Dept. of Chemical Engineering, Indian Institute of Science, Bangalore 560012, India

*DOI 10.1002/aic.12636*
*Published online April 22, 2011 in Wiley Online Library (wileyonlinelibrary.com).*

*Combustion synthesized oxide and vanadate compounds ($CeO_2$, $Fe_2O_3$, $CeVO_4$, and $FeVO_4$) were tested for catalytic hydrogen combustion. The compounds were characterized by X-ray diffraction and X-ray photoelectron spectroscopy. All the four compounds showed good activity and stability for catalytic hydrogen combustion and more than 95% conversion was observed over all the compounds within 500°C. The mechanisms for the reaction over the different classes of compounds (cerium-based and iron-based compounds) were proposed on the basis of spectroscopic observations. The main difference in the mechanisms was in the nature of adsorption of $H_2$ over the sites. The elementary processes for the reaction were proposed, corresponding rate expressions were derived, and the rate parameters for the reaction were estimated using nonlinear regression. Langmuir-Hinshelwood and Eley-Rideal mechanisms were also tested for the reaction and the proposed mechanism was compared with these mechanisms.* © 2011 American Institute of Chemical Engineers *AIChE J,* 58: 932–945, 2012

*Keywords: catalytic hydrogen combustion, mechanism, kinetic models, parameter estimation, catalyst activity, stability*

## Introduction

Hydrogen combustion reaction is a widely used reaction that has several industrial applications. Whereas the direct combustion of $H_2$, referred to as flame combustion, is used in metallurgical industry for the cutting of steel,[1] more recent applications explore its use for combustion along with other fuels in internal combustion engines[2] and gas turbines.[3] Several other industrially important reactions involve the combustion of $H_2$ as one of the associated reactions. Gasification, for example, is a process consisting of a complex set of series-parallel reactions, including $H_2$ combustion.[4,5] In oxidative steam reforming of hydrocarbons and organics, reaction of product $H_2$ with $O_2$ is possible. In case of gasification, flame combustion of $H_2$ takes place while catalytic hydrogen combustion (CHC) is the possibility during steam reforming, and much of the attention has been focused these days on CHC. Preferential oxidation of CO, applied for the purification of $H_2$ stream for fuel cell processors involves oxidation of CO as well as $H_2$ catalytically, and catalysts are developed with an intention of minimizing CHC. Several other chemical systems involve $H_2$ along with other chemical species in which CHC can be expected. Olympiou and Efstathiou have recently reported supported Pt nanocatalysts for $NO_x$ abatement using $H_2$-SCR.[6] Strongly oxidizing conditions are often encountered in such reactions and it may be important to consider CHC as associated reaction.[7,8] Application of $H_2/CO_2$ in bioreactors also imposes the problem of excess $H_2$ which may be required to be processed by CHC and generation as well removal of $H_2S$ depends upon the $H_2$ content and state of the catalyst/adsorbent which is reported

Additional Supporting Information may be found in the online version of this article.

Correspondence concerning this article should be addressed to G. Madras at giridhar@chemeng.iisc.ernet.in

to be influenced by the presence of $H_2$.[9,10] Another important application for CHC is for treatment of exhaust gases from fuel processors/gas turbines, and outlet streams from reactors that operate with excess $H_2$. A detailed description for CHC in different systems and its importance can be found in our previous studies.[11,12]

$H_2$ is known to adsorb dissociatively over Pt. Thus, Pt is an excellent material for CHC and the activity of Pt, as well as other noble metals like Pd, has been reported for CHC.[11–14] However, it is important to understand the role of the support in which the noble metal is dispersed for a better catalyst design. We have previously investigated the water-gas shift reaction over Pd and Pt ions, supported over different supports.[15] It was found that both kinetics as well as mechanism of the reaction differed for different supports, and the support played an important role in the activity of the catalyst. Efstathiou and coworkers[16–19] have also investigated the effect of metal and the support on the kinetics and mechanism of the water-gas shift reaction. Both steady state as well as transient isotope studies by Kalamaras et al.[16,17] have shown the involvement of the support in the reaction with the kinetics of the reaction being governed by the processes at the interface of the metal and the support. Similarly for alumina-based catalysts, active OH/H species were reported to retain on alumina showing the role of the support in the reaction.[18,19] Sharma and Hegde[13] have also compared the activities of different catalysts and have found that different supports showed different rates of reaction. Therefore, it is important to determine the effect of support on the kinetics and mechanism of the reaction, and also explore different materials as potential supports for the reaction. In this study, we have synthesized oxide and vanadate supports viz. $CeO_2$, $CeVO_4$, $Fe_2O_3$, and $FeVO_4$ by solution combustion technique and tested the activity of the supports for CHC without the introduction of any noble metal.

The catalytic activity of $CeO_2$ for oxidation reactions like CO and hydrocarbon oxidation is well reported. The oxygen storage capacity exhibited by $CeO_2$ makes oxygen in the lattice labile and oxidation occurs even in the absence of a noble metal. The reducibility of $CeO_2$ along with the presence of anionic vacancies makes $CeO_2$ an excellent catalytic material.[20] Apart from CO oxidation, $CeO_2$-supported catalysts have been used extensively for the water-gas shift reaction,[21–27] and reforming reactions.[28–30] We have also found high activity of noble metal substituted $CeO_2$ and related solid solutions for CO oxidation and the water-gas shift reaction.[15,31] Following the structure-property relations, the catalysts were tested for CHC and room temperature activity of the catalysts was observed.[11,12] Since the activity of the catalyst is highly dependent upon the support, the current study is intended to explore different supports for the reaction. $Fe_2O_3$ has also been used for the various exhaust catalytic reactions[32–34] and the presence of Fe is reported to influence the catalytic activity of three-way catalysts.[35,36] There are relatively fewer reports on the use of vanadates as supports for catalytic materials. However, vanadates in principle can be good interactive supports owing to the redox couples formed by both V as well as the second metal. Therefore, the catalytic activity of $CeVO_4$ and $FeVO_4$ for CHC was explored.

Vanadium-based catalysts have been reported for numerous oxidation reactions. Mixed oxides of $VO_x$ along with $Al_2O_3$, $ZrO_2$, and $TiO_2$ have been used for oxidation of various organic species.[37–42] $V_2O_5$ has been reported to exhibit a small amount of oxygen storage capacity. But the activation of lattice oxygen is difficult from $O_2$ stream, and the surfaces are inert in the absence of surface reconstructions.[42] We have previously tested the activity of $V_2O_5$ for CO oxidation, and conversions were obtained only on impregnation of Pd.[43] Surface reconstructions with the introduction of Pd and lattice oxygen exchange were found to be responsible for high activity of the catalyst at high temperatures. In vanadates of the type $MVO_4$, where M is a transition or rare earth metal with variable valance, redox couples and electron exchanges between M, V and the reactant species can be expected and, therefore, vanadates can prove to be better supports compared to $V_2O_5$.

This study aimed at exploring different reducible oxides and vanadates for CHC. The use of noble metals in metallic as well as ionic form for the reaction is reported. However, the involvement of the support in the reaction for ionic catalysts for the water-gas shift reaction and CHC has been established in our previous studies.[11,12,15] Therefore, in this study, different supports were used for the reaction and the role of the support for the reaction was established. Support dependent models for describing the course of the reaction were proposed. We have used the spectroscopic observations and the structural analysis of the catalyst for proposing the surface processes taking place during CHC. An analysis of available adsorption sites in the absence of a noble metal was carried out and the corresponding surface processes were proposed. The rate expressions following different models over different compounds were derived from the surface processes and the corresponding rate parameters were estimated.

## Experimental

### *Synthesis and characterization of compounds*

All the compounds were synthesized by solution combustion technique. For the synthesis of $CeO_2$, ceric ammonium nitrate ($(NH_4)_2Ce(NO_3)_6$, Merck, India) was used as the precursor; for the synthesis of $CeVO_4$, ceric ammonium nitrate and ammonium metavanadate ($NH_4VO_3$, S.D. Fine Chem, India) were used as precursors. Similarly, for the synthesis of $Fe_2O_3$, iron (III) nitrate nonahydrate ($Fe(NO_3)_3{\cdot}9H_2O$, S. D. Fine, India) was used as the precursor. Oxalyldihydrazide ($C_2H_6N_2O_4$, Alfa Aesar, India) was used as fuel for all the syntheses. A solution of precursors in deionized water along with the fuel was made and the solution was heated in a muffle furnace preheated at 350°C. The amount of precursors and the fuel were determined by making a balance over the oxidizing and reducing valences.[38] The solution was observed to catch fire after the evaporation of water and the leftover solid was the required compound.

The compounds were characterized by X-ray diffraction (Philips X'pert diffractometer), X-ray photoelectron spectroscopy (Thermo Fisher Scientific Multilab 2000) and $H_2$-temperature programmed reduction. X-ray diffraction was carried out in Phillips X'pert diffractometer. The diffractometer utilized CuK$\alpha$ radiation with a wavelength of 1.5418 nm. The equipment was also equipped with a Ni filter. The

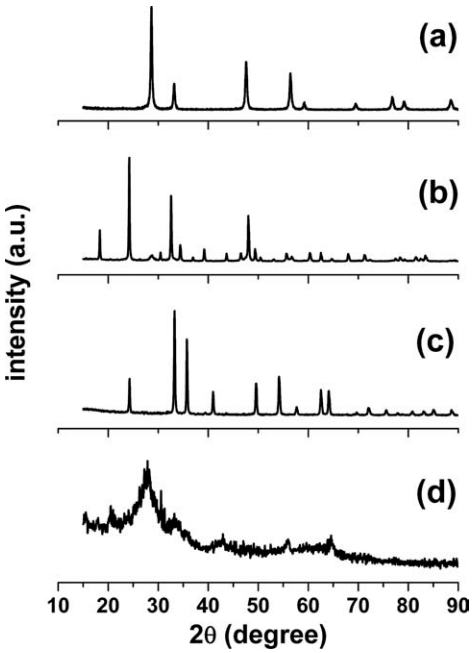


**Figure 1. XRD patterns of combustion synthesized (a) $CeO_2$, (b) $CeVO_4$, (c) $Fe_2O_3$, (d) $FeVO_4$.**

diffraction patterns were recorded in a 2θ range of 15-90o with a step size of 0.017°. X-ray photoelectron spectra (XPS) were recorded on Thermo Fisher multilab spectrophotometer with AlKα radiation which provided energy of 1486 eV. The samples were mixed with a small amount of graphite powder and ground finely. Thin pellets were made and they were mounted in the preparation chamber for degassing for 24 h. The samples in the XPS were etched to remove the surface which is liable to surface oxidation. Therefore, the spectra reported in the study are representative of the bulk catalyst. The spectra were calibrated with reference to C1s observed at a binding energy of 285 eV. XPS were recorded both before and after the reaction for the elucidation of the mechanism of the reaction.

### *Catalytic reactions*

Gas phase catalytic reactions were carried out in 9 mm I.D. glass tube reactors. The reactor was heated using a furnace and the temperature of the furnace was maintained using a PID controller. The catalyst granules were packed between the ceramic wool and the thermocouple was placed in the catalyst bed. Reactions were carried out with different amounts of $O_2$ in the feed maintaining 2.7 vol % $H_2$ and a total flow rate of 100 ml/min. 250 mg of catalyst was used for all the reactions. Analysis of the products were carried out using an online gas chromatogram (Mayura Analytical, Bangalore, India) equipped with Hayesp-A and molecular sieve column, and a thermal conductivity detector. Further details can be found elsewhere.[11,12]

Stability studies were carried out by carrying out the reaction continuously for 12 h. A mixture of $H_2$, $O_2$ and $N_2$ were sent at a total flow rate of 100 ml/min maintaining $H_2$ concentration of 2.7 mol %, $O_2$ concentration of 1.35 mol %. 250 mg of the catalyst was used and a temperature of 500°C was maintained throughout the analysis.

## Results and Discussion

### *Structural studies*

Figure 1 shows the XRD patterns of the synthesized compounds. XRD of $CeO_2$ is shown in Figure 1a. The lines in the pattern can be indexed to the fluorite structure with a space group of *Fm*3*m*. Crystallite size, as calculated by Scherrer formula was found to be 38 nm. $Fe_2O_3$ crystallized in rhombohedral structure with a space group of $R\bar{3}c$ (Figure 1c). The crystallite size was found to be 42 nm. This size is still large compared to that reported using various methods in the literature and ceria crystallites of 10 nm size are common. Nanocrystalline material formation is a characteristic of combustion synthesis[44] and the synthesized compounds in this study were nanocrystalline.

XRD of $CeVO_4$ is shown in Figure 1b. The peaks in the pattern showed the formation of tetragonal $CeVO_4$ with a space group of $I4_1/amd$. The pattern matching was carried out using JCPDF-2 and all the peaks except for the peak of very low intensity 29° showed the formation of tetragonal $CeVO_4$. The impurity peak at 29° was found to correspond to the formation of $CeO_2$. However, the amount of $CeO_2$ in the compound was very small and the compound synthesized was $CeVO_4$. The crystallite size was found to be 41 nm. $FeVO_4$ formation was also confirmed from XRD (Figure 1d). The peaks were very wide and thus reliable crystallite size data could not obtained. However, wide and diffused peaks have been observed by several investigators for $FeVO_4$.[45,46] The compound was found to be triclinic with a space group of $P\bar{1}$ . Ekambaram and Patil[47] have reported the synthesis of a series of vanadates by solution combustion synthesis and triclinic $FeVO_4$ was obtained in their study also.

XPS of Ce3d in $CeO_2$ and $CeVO_4$, before and after CHC with stoichiometric amount of $O_2$ is shown in Figure 2. Ce was found in +4 state in $CeO_2$ and in +3 state in $CeVO_4$. Small peaks in the spectra in the energy range of 892–903 eV can be attributed to the presence of Ce in +4 state. This can be due to the small amounts of $CeO_2$ which was observed in XRD also. Small changes in the oxidation state of Ce can be observed in the spectra after the reaction. A small amount of $Ce^{3+}$ can be observed in the spectra of Ce3d in $CeO_2$ after the reaction. This showed the changes in the oxidation state of Ce in the compound during the reaction, and can be used for probing the mechanism of the reaction. This is discussed in detail in a later section.

Fe in both $Fe_2O_3$ as well as $FeVO_4$ was found to be in +3 states (Figure 3). Fe2p peak position in the spectrum after the reaction was found to shift to lower binding energy. This signified the formation of lower oxidation state and small amounts of $Fe^{2+}$ was formed during the reaction. This also showed the presence of redox $Fe^{2+}$-$Fe^{3+}$ couples during the reaction. A mechanism based upon this observation is proposed in a later section. Vanadium in all the vanadates was in +5 state, and no considerable shifts were observed for different compounds showing the presence of vanadium in +5 states (Figure 4).

Apart from the analysis of the oxidation states of the compounds before and after the reaction, XPS spectra were also

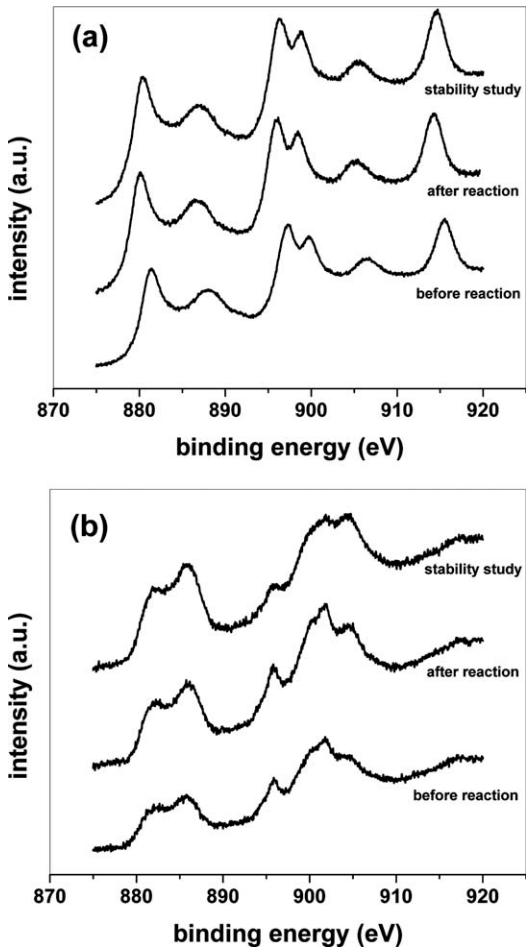


**Figure 2. XPS of Ce3d before and after CHC with stoichiometric amount of $O_2$.**

(a) $CeO_2$, (b) $CeVO_4$.

recorded for the samples treated for testing the stability. CHC was carried out continuously for 12 h over the samples and the spectra of the spent catalyst were recorded. It can be seen in all the spectra that the changes in the oxidation states were similar to the changes observed in the spectra of the compound after the reaction. The conversions for CHC were also monitored (discussed in detail later) and the compounds were found to retain their activity.

### *CHC over different compounds*

Figure 5 shows the variation of $H_2$ conversion with temperature over the different compounds with different amounts of $O_2$ in the feed. All the results can be analyzed in low temperature and high temperature regimes. An exponential increase in conversion with temperature was observed for all the compounds. At higher temperatures, the rates were found to saturate following a sharp light off.

With stoichiometric amount of $O_2$ in the feed ($H_2$:$O_2$ = 2:1), nearly 80% conversion of $H_2$ was observed over $CeO_2$ (Figure 5a). $CeVO_4$ showed relatively higher activity with more than 95% conversion obtained at 400°C (Figure 5b). The activity of $Fe_2O_3$ was relatively lower with only 50% conversion observed at 400°C. However, more than 95% conversion was observed at 500°C. Similarly, more than 95% conversion was observed over $FeVO_4$ also at 500°C.

The effect of $O_2$ on the kinetics of the reaction was studied by increasing the amount of $O_2$ in the feed. The variation of $H_2$ conversion with $O_2$ in the stream two times the stoichiometric requirement ($H_2$:$O_2$ = 1:1) and that corresponding to $O_2$ in air ($H_2$:$O_2$ = 1:7.5) are shown in Figures 5a–d. It can be seen from the figure that with an increase in $O_2$ supply, the conversions increased. For both cerium-based compounds, a decrease in the activity of the catalyst was observed when $O_2$ was used in large excess (air). Possible reason behind this is discussed in a later section. Further, at higher $O_2$ concentrations, the activity of $CeO_2$ was slightly higher than the activity of $CeVO_4$. The changes in the activity with the changes in the temperature and the environment show the combined effect of the reducibility of the compound and the activation of redox couples at different temperatures. The formation of $V_2O_{5-x}$-type species in $CeVO_4$ is detrimental for the activity of the compound and similar

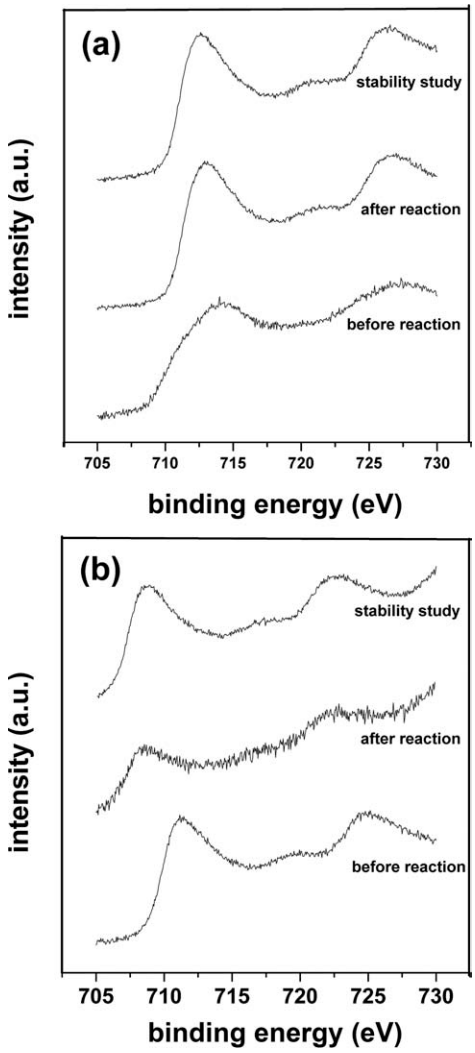


**Figure 3. XPS of Fe2p before and after CHC with stoichiometric amount of $O_2$.**

(a) $Fe_2O_3$, (b) $FeVO_4$.

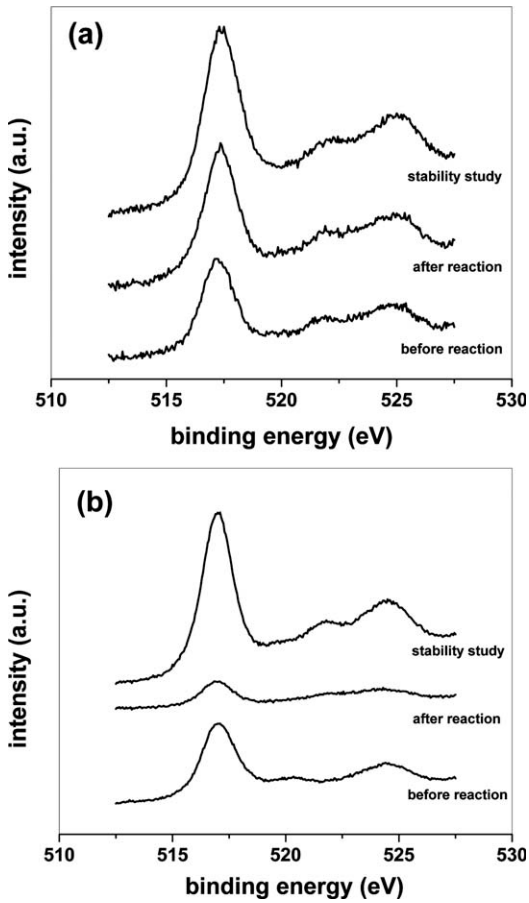


**Figure 4. XPS of V2p before and after CHC with stoichiometric amount of $O_2$.**

(a) $CeVO_4$, (b) $FeVO_4$.

phenomena has been observed during $H_2$-SCR reactions.[48] In oxygen rich environment at lower temperatures, the formation of $V_2O_{5-x}$-type species is likely due to oxidizing conditions. However, at higher temperatures, the rates of redox couple formation can be expected to increase resulting in enhanced activity of the compound for the reaction. The enhancement in the activity with an increase in $O_2$ supply was found to be the highest when the reaction was carried out over $FeVO_4$. It can be seen from Figure 5d that nearly complete conversions were obtained below 150°C when excess of $O_2$ was used. A sharp light off was be observed at higher $O_2$. In general, a sigmoidal dependence of conversion of $H_2$ on temperature was observed showing the presence of mass transfer limitations at very high temperatures.

### *Modeling CHC over different compounds*

We model the reaction on the basis of the structure of the compound and the spectroscopic observations. $CeO_2$ is a reducible oxide, and nonstoichiometry of the oxide has been established by several techniques, including $H_2$-uptake measurements.[20] Lattice oxygen exchange in reducing atmosphere is possible in $CeO_2$ resulting in reduced ceria. Therefore, during CHC, the following reactions are possible

$$Ce^{4+}O_2^{2-} + \delta H_2 \rightarrow Ce_{2\delta}^{3+}Ce_{1-2\delta}^{4+}O_{2-\delta}^{2-} + \delta H_2O \quad (1)$$

$$Ce_{2\delta}^{3+}Ce_{1-2\delta}^{4+}O_{2-\delta}^{2-} + \left(\delta/2\right)O_2 \rightarrow Ce^{4+}O_2^{2-} \quad (2)$$

$\delta$ in the equations is the oxygen storage capacity, and determines the extent of reduction of $CeO_2$ to reduced ceria. High values of $\delta$ are desirable for high activity of the catalyst. Equation 1 shows the interaction of $H_2$ with $CeO_2$ resulting in the loss of lattice oxygen that results in the formation of $H_2O$ and a corresponding reduction of $CeO_2$. A part of $Ce^{4+}$ gets reduced to $Ce^{3+}$. This process may result in the formation of anionic vacancies, implications of which are discussed later. Reduced ceria can get oxidized to $CeO_2$ by the interaction with $O_2$ from the stream. This is shown by Eq. 2.

The temperature at which $CeO_2$ reduction takes place can be determined by $H_2$-uptake measurements. We have previously found room temperature CHC activity of Pd/Pt substituted $CeO_2$.[12] Both adsorption of $H_2$ as well as the reducibility of $CeO_2$ are enhanced by the presence of a metal ion. However, unsubstituted $CeO_2$ reduces around 300°C, and, hence, the activity of $CeO_2$ for CHC can be expected at relatively higher temperatures compared to that shown by metal substituted catalysts. $CeO_2$ was indeed found to be active for CHC and more than 98% conversions were observed over $CeO_2$, as can be seen from Figure 5.

$Fe_2O_3$ $H_2$-TPR also showed reduction peaks at temperatures above 350°C (see Supporting Information Figure S1a). Therefore, $Fe_2O_3$ is also liable to get reduced by $H_2$ and can act as a CHC catalyst. Reduction of $Fe_2O_3$ by $H_2$ can take place via the following reactions

$$Fe_2O_3 + H_2 \rightarrow 2FeO + H_2O \quad (3)$$

$$FeO + H_2 \rightarrow Fe + H_2O \quad (4)$$

However, the above set of equations show complete reduction of Fe and a large amount of lattice oxygen removal is very unlikely at lower temperature (below 600°C). Further, Fe metal was not observed in the XPS of the catalysts after the reactions, whereas a mixed oxidation state of +2/+3 was observed. Therefore, like $CeO_2$, only a partial reduction of $Fe_2O_3$ is possible and the following reactions can be expected to be taking place during CHC.

$$Fe_2^{3+}O_3^{2-} + \delta H_2 \rightarrow Fe_{2\delta}^{2+}Fe_{2-2\delta}^{3+}O_{3-\delta}^{2-} + \delta H_2O \quad (5)$$

$$Fe_{2\delta}^{2+}Fe_{2-2\delta}^{3+}O_{3-\delta}^{2-} + \left(\delta/2\right)O_2 \rightarrow Fe_2^{3+}O_3^{2-} \quad (6)$$

Equation 5 shows the reduction of Fe from $Fe^{3+}$ to $Fe^{2+}$ by the loss of lattice oxygen. Gain of lattice oxygen is shown by Eq. 6 in which oxygen from the stream is utilized for the oxidation of reduced iron oxide.

Vanadates of cerium and iron have also been found to be reducible. Reduction of $CeVO_4$ takes place above at 400°C[49] whereas $FeVO_4$ shows reduction above 425°C (Supporting Information Figure S1b). Therefore, analogous to lattice oxygen exchange in $CeO_2$ and $Fe_2O_3$, lattice oxygen exchange is possible in vanadates of corresponding metals. However, the extent of reducibility and the activities of different vanadates may be different.

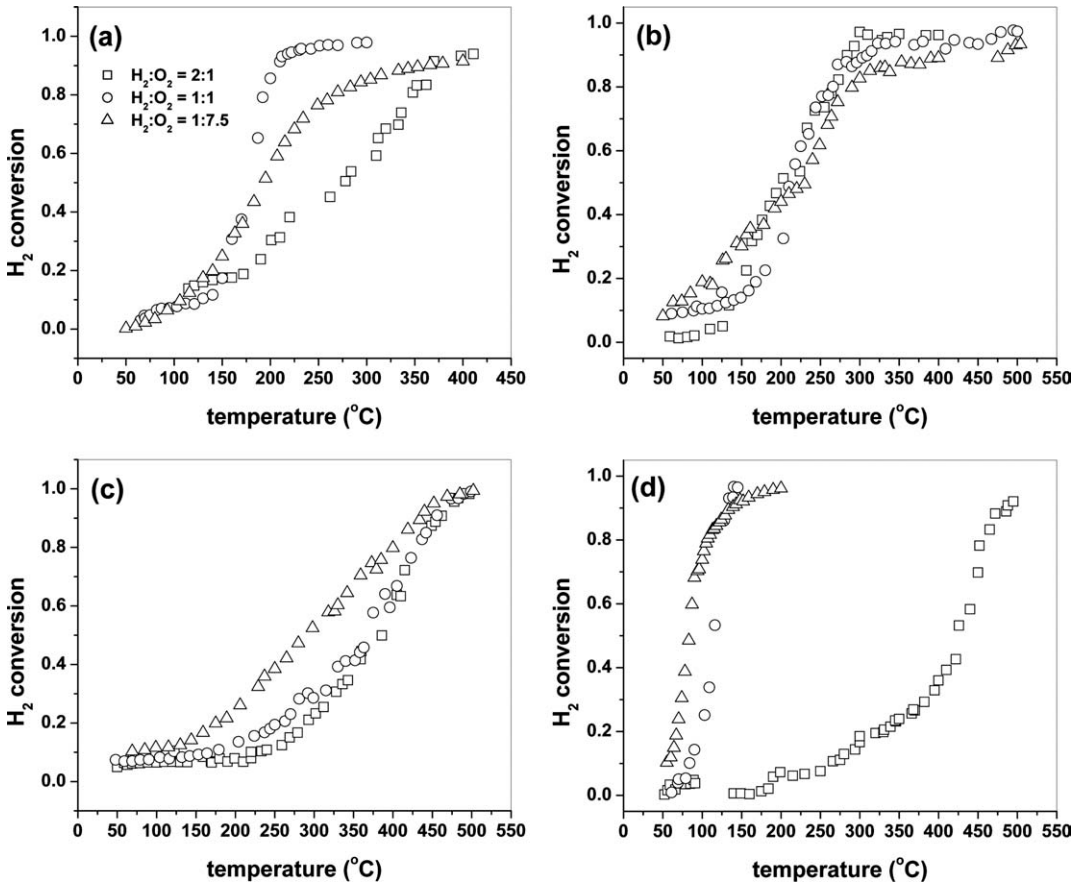


**Figure 5. Variation of $H_2$ conversion with temperature over (a) $CeO_2$, (b) $CeVO_4$, (c) $Fe_2O_3$, (d) $FeVO_4$.**

The presence of V in vanadates can induce additional redox couples in the compound by interactions with the second metal. As a result, enhanced activity can be expected due to electron exchanges among the various species. In both $CeVO_4$ as well as $FeVO_4$, V was found in +5 state, as confirmed by XPS (Figure 4). Ce and Fe were found to be in +3 state (Figures 2 and 3). These oxidation state combinations result in differences in the behavior of $CeVO_4$ and $FeVO_4$. Fe in $FeVO_4$ was in +3 state and reduction to +2 state is feasible. But, reduction of Ce from +3 state in $CeVO_4$ is very unlikely. Therefore, reduction of $Fe^{3+}$ to $Fe^{2+}$ can take place in $FeVO_4$. Reduction of $V^{5+}$ to $V^{4+}$ is required in $CeVO_4$.

$$Fe^{3+}V^{5+}O_4^{2-} + \delta H_2 \rightarrow Fe^{2+}_{2\delta}Fe^{3+}_{1-2\delta}V^{5+}O^{2-}_{4-\delta} + \delta H_2O \quad (7)$$

$$Fe^{2+}_{2\delta}Fe^{3+}_{1-2\delta}V^{5+}O^{2-}_{4-\delta} + \left(\delta/2\right)O_2 \rightarrow Fe^{3+}V^{5+}O_4^{2-} \quad (8)$$

Equation 7 shows the reduction a partial reduction of $Fe^{3+}$ in $FeVO_4$ to $Fe^{2+}$ following lattice oxygen loss. Reoxidation by $O_2$ from the stream is shown by Eq. 8. However, as mentioned earlier, partial reduction of $V^{5+}$ to $V^{4+}$ is indeed possible and the following can be written

$$Fe^{2+}_{2\delta}Fe^{3+}_{1-2\delta}V^{5+}O^{2-}_{4-\delta} \leftrightarrow Fe^{2+}_{x}Fe^{3+}_{1-x}V^{4+}_{y}V^{5+}_{1-y}O^{2-}_{4-\delta} \quad (9)$$

where

$$x + y = 2\delta \quad (10)$$

Equation 9 shows the rearrangement of the electronic states of Fe and V by electron exchanges during the reaction. The relative values of x and y depend upon the reducibility of the compound.

Unlike $FeVO_4$, the analogous reaction for the reduction of Ce can not be written as Ce is present in +3 state in $CeVO_4$. Therefore, reduction of the compound with $H_2$ can be written as follows

$$Ce^{3+}V^{5+}O_4^{2-} + \delta H_2 \rightarrow Ce^{3+}V^{4+}_{2\delta}V^{5+}_{1-2\delta}O^{2-}_{4-\delta} + \delta H_2O \quad (11)$$

Reoxidation by $O_2$ stream is given by

$$Ce^{3+}V^{4+}_{2\delta}V^{5+}_{1-2\delta}O^{2-}_{4-\delta} + \left(\delta/2\right)O_2 \rightarrow Ce^{3+}V^{5+}O_4^{2-} \quad (12)$$

The electron exchanges and changes in the oxidation states are given by the following relations

$$Ce^{3+}V^{4+}_{2\delta}V^{5+}_{1-2\delta}O^{2-}_{4-\delta} \leftrightarrow Ce^{3+}_{1-x}Ce^{4+}_{x}V^{4+}_{y}V^{5+}_{1-y}O^{2-}_{4-\delta} \quad (13)$$

$$y - x = 2\delta \quad (14)$$

From Eq. 14, it can be clearly seen that the reduction of V is greater than the oxidation of Ce, since $\delta$ has to be positive. This shows that Ce is very stable in +3 state in $CeVO_4$, and, therefore, the changes in the oxidation state are

relatively difficult compared to the changes in the oxidation state of Fe in $FeVO_4$.

On the basis of the above discussion, the mechanism of CHC can be deduced. It can be seen that all the compounds are reducible and the exchange of the lattice oxygen takes place. Replenishment of the lattice oxygen takes place from the stream oxygen. Therefore, a common reaction mechanism can be proposed for CHC over all the four compounds consisting of the following processes:

(a) adsorption of $H_2$ over a suitable site in the compound

(b) reduction of the support and formation of $H_2O$

(c) splitting of $O_2$ from the stream and reoxidation of the support.

Depending upon the relative magnitudes of the different steps over different compounds, the rates of the reaction may vary. We analyze all the three steps individually over all the compounds and propose a mechanism for the reaction.

*Adsorption of $H_2$.* In case of noble metal impregnated or substituted compounds, noble metal sites act as sites for adsorption of $H_2$. However, even in the absence of noble metals, the compounds showed activity of CHC. $O_2$ is known to adsorb and dissociate over the defect sites and the involvement of support in the reaction is through the sites for dissociative adsorption of $O_2$ over the defect sites. This is particularly true for reducible oxides like $CeO_2$, and the presence of dual site mechanism for CO oxidation has been proved for noble metal ion-substituted catalysts.[31] Therefore, the main issue to be addressed for catalysis in the absence of metals is the availability of adsorption sites for $H_2$. One of the possibilities is the presence of Eley-Rideal type mechanism for the reaction in which $H_2$ can react from the gas phase and $O_2$ can react from the adsorbed phase. However, TPR have indeed shown $CeO_2$ to be a compound with large chemisorption of $H_2$. $CeO_2$ is shown to chemisorb $H_2$ by two ways; one reversibly as $H_2$ and another irreversibly as $H_2O$. Studies by Bernal et al.[50] have shown that chemisorption of $H_2$ over $CeO_2$ takes place resulting in reduced ceria, and the center of adsorption being mainly oxygen ions, although small contributions for $Ce^{3+}$ centers can also be expected. A study by Zafiris and Gorte[51] has shown that the adsorption of $H_2$ over Pt, dispersed in $CeO_2$ as well as $Al_2O_3$ remains the same, independent of the support identity. This clearly shows that the contribution from Ce ions is not significant for the adsorption of $H_2$. However, adsorption over $CeO_2$ has been reported to be an activated process, the rate of adsorption being higher at higher temperature.[52] Chemisorption of $H_2$ over $CeO_2$ can lead to the formation of either hydroxyl species or hydride species. IR spectroscopic studies have revealed the formation of hydroxyl groups during chemisorption. We have also observed changes in the XPS signals before and after reaction for $CeO_2$ samples. Therefore, it can be concluded that even in the absence of a metal ion, $CeO_2$ can indeed provide centers for chemisorption of $H_2$.

Adsorption of $H_2$ over $Fe_2O_3$ is also reported to be an activated process with nondissociative adsorption of $H_2$ taking place over Fe ions.[53] A study by Rodriguez et al.[53] has shown that chemisorption of $H_2$ over Fe in $Fe_2O_3$ weakens H—H bond, however, keeping the molecule intact. This is in contrast to the adsorption of $H_2$ over $CeO_2$, where not only the adsorption centers are oxygen ions, but also the adsorption takes place dissociatively.

There are no reports on the adsorption of $H_2$ over $CeVO_4$ or $FeVO_4$. However, the adsorption centers over these compounds are be considered to be similar to those present in $CeO_2$, or $Fe_2O_3$. Adsorption involves electrostatic interactions between the adsorbent and the adsorbate. Therefore, adsorption differs for the adsorbent with different oxidation states. Since Fe was present in +3 state in both $Fe_2O_3$ as well as $FeVO_4$, and adsorption centers were Fe ions, the same expression was used for the adsorption of $H_2$ over both the compounds. However, since no reports were available for the adsorption of $H_2$ over $CeVO_4$ or $Ce^{3+}$ ions, the expression for adsorption over $CeO_2$ was used as an approximation for the adsorption of $H_2$ over $CeVO_4$. Therefore, the underlying assumption in the analysis of the reaction over $CeVO_4$ and $FeVO_4$ is the similarity in the adsorption sites for $H_2$ over the corresponding oxides.

*Reduction of Support and the Formation of $H_2O$.* After the adsorption of $H_2$ over the support, reduction of the support over all the compounds takes place in a similar manner. Utilization of the lattice oxygen from the support from the adsorbed hydrogen, either in the form of hydroxyl groups or adsorbed molecular $H_2$, takes place. The interaction of hydrogen and the lattice oxygen results in the formation of $H_2O$. This phenomenon can be expected to be similar over all the compounds. The rates of this particular step can differ due to the differences in the reducibility of the compounds. Both, the ease of lattice oxygen exchange, as well as the extent of lattice oxygen exchange will determine the activity of the compound for CHC.

*Splitting of $O_2$ from the Stream and Reoxidation of the Support.* This particular step is also expected to be similar over the different supports as long as the reduction of the support takes following the equations previously proposed. Due to bulk changes in the structure required for complete reduction of $CeO_2$ to $Ce_2O_3$ or $Fe_2O_3$ to FeO, complete reduction of the support does not take place. Partial reduction, resulting in the formation of $Ce^{4+}/Ce^{3+}$ and $Fe^{3+}/Fe^{2+}$ in the compounds, results in the formation of anionic vacancies. These anionic or oxygen ion vacancies act as dissociative adsorption sites for $O_2$ from the stream. This phenomenon is known and reported for the reactions like CO oxidation and also for the dissociation of $H_2O$ for the case of the water-gas shift reaction.[15,33] This particular step is unique only for the case of reducible oxides in which the splitting of the oxygen takes place on oxygen deficient sites. This step results in the reoxidation of the support by utilization of a part of $O_2$ from the stream. For the case of nonreducible oxides like $Al_2O_3$ or $ZrO_2$ also, the defect sites can result in the dissociative adsorption of $O_2$. However, it is to be noted that no utilization of lattice oxygen takes place in such oxides, and the dissociated oxygen is utilized for the oxidation of $H_2$. Depending upon the nature of the sites, the sites can also act as adsorption sites of $H_2$ and therefore, a sequential single site mechanism can be expected over such oxides. However, in the present case, clearly two different sites are required for the adsorption of $H_2$ and dissociative adsorption of $O_2$.

Based upon the above analyses of the various steps involved during CHC, we propose two different mechanisms

for CHC over the two classes of compounds. For cerium-based compounds, we propose dissociative adsorption mechanism, and for iron-based compounds, we propose molecular adsorption mechanism.

### *Dissociative adsorption mechanism for cerium-based compounds*

Various processes taking place during CHC over cerium-based compounds ($CeO_2$ and $CeVO_4$) are shown in Scheme 1, and the associated reactions can be written as follows

$$H_2 + 2S - CeO \leftrightarrow 2S - H - CeO \quad (15)$$

$$2S - H - CeO + O_L \rightarrow H_2O + S - CeO + S - CeR - v \quad (16)$$

$$S - CeR - v + O_2 \rightarrow S - CeO \cdot O + O_L \quad (17)$$

$$S - CeO \cdot O + H_2 \rightarrow H_2O + S - CeO \quad (18)$$

Dissociative adsorption of $H_2$ takes place over oxygen ions in the compound. This is shown in Eq. 15. Dissociation and spillover of H to the adjacent vacant oxygen ion is shown as a single step. $S - CeO$ in Eq. 15 is the adsorption site in the compound where CeO signifies the oxidized cerium compound. By the interaction of similar adjacent site, dissociation and spillover of H takes place.[50] The sequential step can be shown as the following

$$H_2 + s - CeO \leftrightarrow S - H_2 - CeO \overset{s-CeO}{\longrightarrow} S - H - CeO \quad (19)$$

But it is found that depending upon the reduction temperature, only one of the two steps in Eq. 19 is limiting. Spillover results in the formation of surface hydroxyl groups, which are well observed and reported. Equation 16 shows the lattice oxygen utilization, resulting in the release of $H_2O$. $O_L$ represents the lattice oxygen in the compound and its concentration is signified as the amount of labile oxygen in the compound in the proximity of adsorbed H species, which is given out by the compound during the reaction. Owing to the loss of lattice oxygen, anionic vacancies are formed. $S - CeR - v$ in the equation shows the reduced form of the compound with anionic vacancies. Release of $H_2O$ will result in vacating one of the sites for $H_2$ adsorption, while the vacancy will be formed in the other site. Dissociation of $O_2$ over these vacancies is shown in Eq. 17. Dissociative adsorption of $O_2$ over the vacancies has been observed using infrared spectroscopic studies. Lambrou et al.[35] have detected the different oxygen species and their transition to different forms using infrared spectra. Initial dioxygen species was observed to transform to oxygen species over the vacant sites via the formation of intermediate superoxide and peroxide species. One of the oxygen atoms of the oxygen molecule is utilized for the reoxidation of the compound and the second atom is retained on the support as weakly bonded oxygen species. This weakly bonded oxygen species can interact directly with $H_2$ from the stream to release $H_2O$ and restore the original catalyst. This is shown in Eq. 18. It is important to note here that the interaction of the surface bonded oxygen with the dissociated hydrogen species in the catalysts requires simultaneous interactions among more than three sites for the formation of $H_2O$ and, hence, such a step is not possible. The only way that the complete catalytic cycle takes place, consistent with the stoichiometry, and the fundamental surface processes is the proposed way in which hydrogen is utilized both from adsorbed phase as well as from the gas phase. The above proposed mechanism can be considered to be modified Eley-Rideal mechanism in which $O_2$ reacts from the adsorbed phase while $H_2$ reacts from both adsorbed as well as gas phase.

The rate expression derived on the basis of the reactions (15) to (18) can be written as follow

$$r_{H_2} = \frac{2k_{17}k_{18}[H_2][O_2]}{k_{17}[O_2] + k_{18}[H_2]} \quad (20)$$

The details of the derivation and the underlying assumptions can be found in Appendix A.

### *Molecular adsorption mechanism for iron-based compounds*

As mentioned earlier, adsorption of $H_2$ over $Fe_2O_3$ takes place nondissociatively with Fe ions as adsorption centers. The mechanism for CHC over iron-based compounds differs from that over cerium-based compound in this particular step. The adsorption kinetics can have an influence over the overall reaction kinetics and, therefore, a different mechanism is proposed for iron-based compounds. The detailed scheme for the reaction is shown in Scheme 2. Related equations for the mechanism can be written as follows

$$H_2 + S - FeO \leftrightarrow S - H_2 - FeO \quad (21)$$

$$S - H_2 - FeO + O_L \rightarrow H_2O + S - FeR - v \quad (22)$$

$$O_2 + S - FeR - v \rightarrow S - FeO \cdot O + O_L \quad (23)$$

$$H_2 + S - FeO \cdot O \rightarrow H_2O + S - FeO \quad (24)$$

Molecular adsorption of $H_2$ over Fe ions is shown by Eq. 21. The adsorbed species is shown by $S - H_2 - FeO$. It is important to note here that FeO in the equation is only a notation for oxidized iron site and does not denote iron (II) oxide. Molecularly adsorbed $H_2$ in the compound abstracts oxygen from the lattice, resulting in the release of $H_2O$ and reduced iron oxide with vacancies, denoted as $S - FeR - v$. This is shown in Eq. 22. Equations 23 and 24 are the equations analogous to Eqs. 18 and 19, showing the dissociation of $O_2$ over the oxygen ion vacancies, reoxidation of the support, formation of weakly adsorbed oxygen species on the support, interaction of $H_2$ from gas phase with oxygen adsorbed in the support, and release of $H_2O$ giving back the catalyst in its original form. The rate expression for the set of reactions following Eqs. 21–24 can be written as follows

$$r_{H_2} = \frac{2k_{23}k_{24}[H_2][O_2]}{k_{23}[O_2] + k_{24}[H_2]} \quad (25)$$

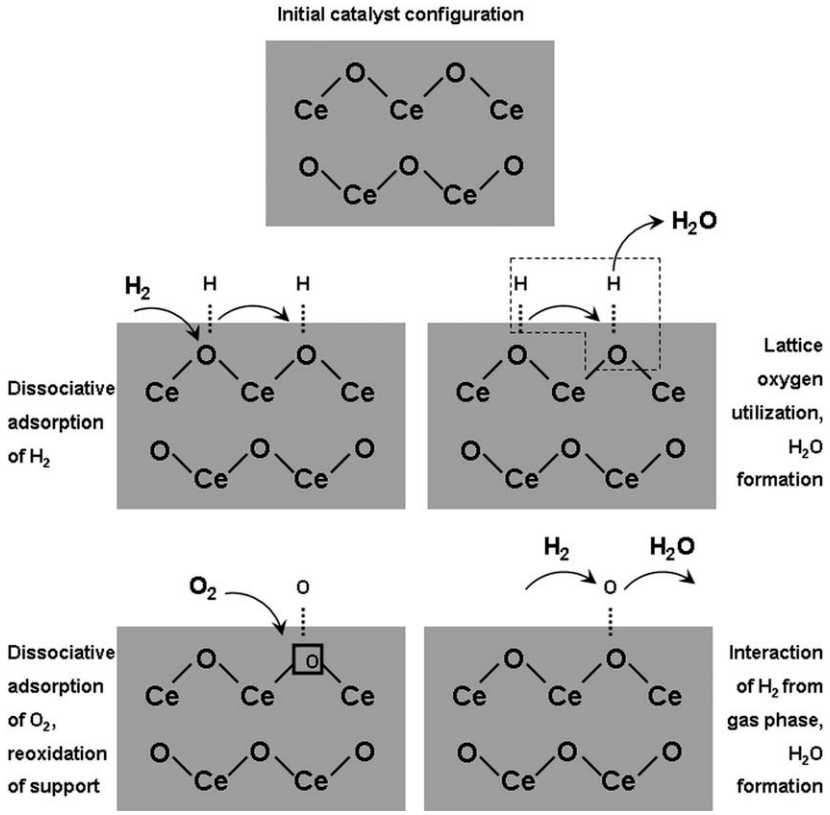


**Scheme 1. Mechanism of CHC over cerium-based compounds.**

Identical forms for the rate of reaction can be observed from Eqs. 20 and 25. It is important to note that the rate expression involves the rate coefficients involving the lattice oxygen utilization and interaction of $H_2$ with surface oxygen species. This clearly shows that the rate of reaction is surface reaction limited and $H_2$ adsorption has is not a rate controlling step. We have previously observed similar phenomena for the water-gas shift activity of $CeO_2$-based compounds.[54]

### *Model validation and parameter estimation*

The rate coefficients appearing in Eqs. 20 and 25 were determined using nonlinear regression for the data given in Figure 5. The rate coefficients were written as temperature dependent quantities using Arrhenius equation

$$k_i = A_i \exp(-E_i/RT) \tag{26}$$

where $A_i$ are the pre-exponential factors, $E_i$ are the activation energies, and $i$ is the index of the corresponding reaction. The variation of conversion with temperature was expressed using the rate equations and rate equation for a flow reactor based upon appropriate material balance. The relation for iron-based catalysts, for example, was written as

$$x_{H_2} = \frac{W}{F_{H_2}} \left( \frac{2A_{23} \exp(-E_{23}/RT) A_{24} \exp(-E_{24}/RT)[H_2][O_2]}{A_{23} \exp(-E_{23}/RT)[O_2] + A_{24} \exp(-E_{24}/RT)[H_2]} \right) \tag{27}$$

The above expression gives the variation of conversion with temperature. $W$ and $F_{H_2}$ in the above equation represent the catalyst loading and molar flow rate of $H_2$, respectively. The quantities in the above equation were determined by minimizing the square of the difference between the experimental and observed conversions. The actual values of the rates were not quantified and instead, the relation between rate and conversion was used for the direct regression of conversion and the rate parameters were determined using the $H_2$ conversion data.

The rate parameters following the two different models are shown in Table 1. Figure 6 shows the predicted values of conversion corresponding to the experimental values of the conversion. The closeness of the points around the line at 45° to the horizontal gives the idea about the goodness of the fit. It can be observed from Figure 6 that the models could describe the process well, as signified by the concentration of the points close to the line. For Eq. 27 to be valid, the reactor has to be operated under differential conditions. This is true for lower conversions and, therefore, only lower conversions were used for regression. At higher conversions, the predictions of the model were not accurate, as can be seen from a large scatter in the data at higher conversions. Equation 27 assumes well mixed conditions in the reactor. With an increase in the conversion and the amount of catalyst, well mixed conditions may no longer exist. Further, it should be noted that a sharp light off was observed for the reaction at higher catalyst concentrations and $O_2$ supply. Therefore, the assumption of well mixed system breaks

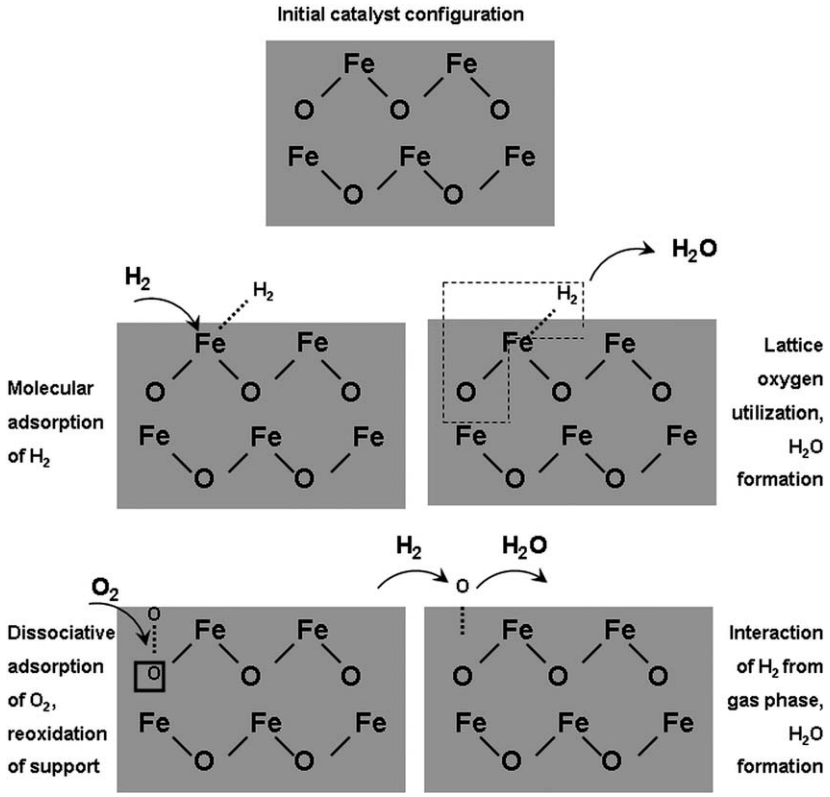


**Scheme 2. Mechanism of CHC over iron-based compounds.**

down and the further analysis may be required. Further, the kinetic analysis was possible only for case when stoichiometric amount of $O_2$ was used in the feed. As can be seen in Figure 5, the conversions were very high with higher amounts of $O_2$ and the assumptions used for determining the rate parameters can no longer be used. Therefore, it may not be possible to verify or extend the results of regression for the reaction systems utilizing higher amounts of $O_2$ in the current case. However, the reaction can be carried out with higher space velocities so as to obtain low enough conversions such that the data can be used for quantitative kinetic analysis. Difference on the behavior of $CeO_2$ at higher $O_2$ or very high activity of $FeVO_4$ may require further investigation for the mechanism of the reaction.

### *Comparison with standard models for heterogeneous catalytic reactions*

We also present a comparison of the proposed model with the standard models for heterogeneous catalysis reported in the literature viz., Eley-Rideal model and Langmuir-Hinshelwood model.

*Eley-Rideal Mechanism.* This mechanism assumes the reaction to take place via the adsorption of one of the species on the active sites, interaction of the adsorbed species with the second species in gas phase, the second species being not adsorbed over the catalyst, surface reaction and release of the products. The steps for the mechanism can be written as follows

$$O_2 + 2S \leftrightarrow 2O - S \tag{28}$$

$$H_2 + O - S \rightarrow H_2O + S \tag{29}$$

Equation 28 represents the dissociative adsorption of $O_2$ on the adsorption sites to give surface oxygen species. $H_2$ from the gas phase can react with adsorbed oxygen to release $H_2O$. The rate expression corresponding to Eqs. 28 and 29 can be written as

$$r_{H_2} = \frac{k_{29}[H_2]\sqrt{K_{28}[O_2]}}{1 + \sqrt{K_{28}[O_2]}} \tag{30}$$

The details of derivation of Eq. 30 can be found in Appendix C.

*Langmuir-Hinshelwood Mechanism with Dissociative Adsorption of $H_2$.* In this mechanism, both $H_2$ as well as $O_2$ are assumed to adsorb dissociatively over the sites to gives surface species. The interaction of the surface species result in the formation of $H_2O$. The steps for the reaction can be written as follows

**Table 1. Rate Parameters for the Variation of $H_2$ Concentration with Time Following the Different Mechanisms**

| | $k_{17}$ | $k_{18}$ |
|---|---|---|
| $CeO_2$ | 13exp(−2657/T) | 27,137exp(−3768/T) |
| $CeVO_4$ | 952exp(−2070/T) | 2435exp(−3104/T) |
| | $k_{23}$ | $k_{23}$ |
| $Fe_2O_3$ | 238exp(−5204/T) | 3346exp(−4626/T) |
| $FeVO_4$ | 41963exp(−8291/T) | 1861exp(−5026/T) |

Frequency factors in mol/(gs); activation energies in kJ/mol.

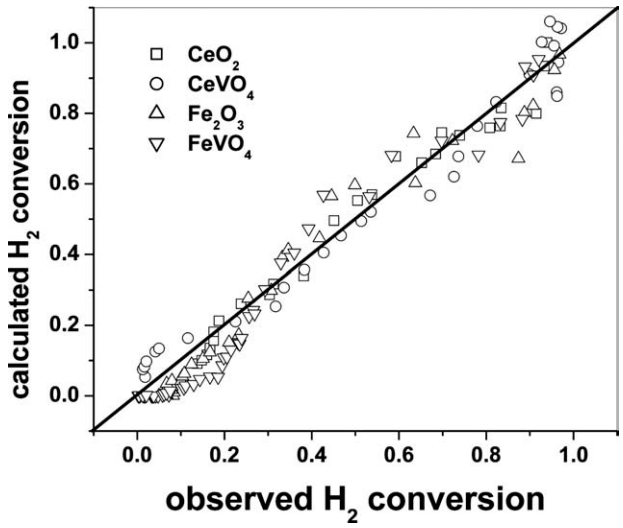


**Figure 6. Experimental and calculated $H_2$ conversions over different catalysts.**

$$H_2 + 2S \leftrightarrow 2H - S \tag{31}$$

$$O_2 + 2S \leftrightarrow 2O - S \tag{32}$$

$$2H - S + O - S \rightarrow H_2O + 3S \tag{33}$$

As discussed earlier, adsorption of $H_2$ over cerium-based compounds takes place dissociatively. Therefore, dissociative step has been used in Eq. 32. The dissociative adsorption of $H_2$ and $O_2$ are shown by Eqs. 31 and 32, respectively. The interaction of the surface $H - S$ and $O - S$ species to give $H_2O$ is shown by Eq. 33. The rate expression for the set of reactions 31–33 can be written as

$$r_{H_2} = \frac{k_{33}K_{31}\sqrt{K_{32}}[H_2]\sqrt{[O_2]}}{\left(1 + \sqrt{K_{31}[H_2]} + \sqrt{K_{32}[O_2]}\right)^3} \tag{34}$$

The details of the derivation can be found in Appendix C.

*Langmuir-Hinshelwood Mechanism with Molecular Adsorption of $H_2$.* Adsorption of $H_2$ over Fe-based compounds takes place molecularly. Therefore, this mechanism involves molecular adsorption of $H_2$ and dissociative adsorption of $O_2$ over the sites, and the interaction of the surface species to release $H_2O$. The equation for the steps can be written as follows

$$H_2 + S \leftrightarrow H_2 - S \tag{35}$$

$$O_2 + 2S \leftrightarrow 2O - S \tag{36}$$

$$H_2 - S + O - S \rightarrow H_2O + 2S \tag{37}$$

The rate expression for the above set of reactions is given by Eq. 38. The details of the derivation are given in Appendix C.

$$r_{H_2} = \frac{k_{37}K_{35}[H_2]\sqrt{K_{36}[O_2]}}{\left(1 + K_{35}[H_2] + \sqrt{K_{36}[O_2]}\right)^2} \tag{38}$$

The regression plot for $H_2$ combustion following Eley-Rideal mechanism is shown in Figure S3 (see Supporting Information). It can be seen from the regression plot that for all the catalysts, the predicted conversions were not in agreement with the observed $H_2$ conversions. Where as a large scatter in the data can be observed at high conversions, the model completely underpredicted conversions at lower conversions. Almost no conversion is predicted by the model when the observed conversions were as high as 20%. Therefore, Eley-Rideal mechanism can not be considered to correctly describe the mechanism of the reaction. When Langmuir-Hinshelwood mechanism was for tested for describing the reaction, either no convergence in the regression was observed or physically unacceptable parameters were observed.

### *Stability studies*

Fresh catalysts were used for carrying out stability studies. The reaction was carried out for nearly 600 min continuously and the variation of $H_2$ concentration with time was observed. This is shown in Figure S2 (see Supporting Information). It can be observed that for all the catalysts, no considerable decrease in the activity takes place. Only $Fe_2O_3$ showed nearly 15% decrease in the activity. A possible reason can be sintering of the catalyst resulting in the loss of surface area as no considerable changes in the electronic structure of the catalyst were observed, as confirmed by the XPS of the spent catalyst. For the rest of the catalysts, the decrease in the activity was lesser than 5%. However, major changes in the XPS of Fe and V can indeed be observed after long time exposure of $FeVO_4$ (Figures 3b and 4b). Therefore, $FeVO_4$ can potentially show deactivation if the exposure is continued for a longer time.

## Conclusions

Both oxide as well as vanadate supports showed high activity for CHC in the 250–500°C range. The rates of reaction were very high when the reaction was carried out with high concentrations of $O_2$ in the stream. $FeVO_4$ was found to be the best catalyst. The possible reason behind the high activity of the compound was the presence of favorable $Fe^{3+}$-$Fe^{2+}$ and $V^{5+}$-$V^{4+}$ redox couples. Reaction was found to proceed via dissociative $H_2$ adsorption mechanism over ceria-based compounds while it was found to proceed via molecular adsorption over iron-based catalysts.

## Acknowledgments

P.A.D. thank Bristol-Myers Squibb for the graduate fellowship, G.M. thank the Department of Science and Technology for the Swarnajayanti fellowship.

## Literature Cited

1. Tusek J, Sraj M. Oxy-hydrogen flame for cutting of steel. *Metallurgica*. 2007;46:663–647.
2. Senthil Kumar M, Ramesh A, Nagalingam B. Use of hydrogen to enhance the performance of a vegetable oil fuelled compression ignition engine. *Int J Hydrogen Energy*. 2003;28:1143–1154.
3. Lee MC, Seo SB, Chung JH, Kim SM, Joo YJ, Ahn DH. Gas turbine combustion performance test of hydrogen and carbon monoxide synthetic gas. *Fuel*. 2010;89:1485–1491.

4. Wurzenberger JC, Wallner JC, Raupenstrauch H, Khinast JG. Thermal conversion of biomass: comprehensive reactor and particle modeling. *AIChE J*. 2002;48:2398–2411.
5. Radmanesh R, Chaouki J, Guy C. Biomass gasification in a bubbling fluidized bed reactor: experiments and modeling. *AIChE J*. 2006; 52:4258–4272.
6. Olympiou GG, Efstathiou AM. Industrial $NO_x$ control via $H_2$-SCR on a novel supported-Pt nanocatalyst. *Chem Eng J*. Published online; DOI: 10.1016/j.cej.2011.01.001.
7. Savva PG, Costa CN, Efstathiou AM. The mechanism of reduction of NO with $H_2$ in strongly oxidizing conditions ($H_2$-SCR) on a novel Pt/MgO-$CeO_2$ catalyst: effects of reaction temperature. *Kinetics Catal*. 2008;49:743–747.
8. Savva PG, Efstathiou AM. The influence of reaction temperature on the chemical structure and surface concentration of active $NO_x$ in $H_2$-SCR over Pt/MgO-$CeO_2$: SSITKA-DRIFTS and transient mass spectrometry studies. *J Catal*. 2008;257:325–333.
9. Polychronopoulou K, Efstathiou AM. Effects of sol-gel synthesis on 5Fe-15Mn-40Zn-40Ti-O mixed oxide structure and its $H_2S$ removal efficiency from industrial gas mixture. *Environ Sci Technol*. 2009; 43:4367–4372.
10. Polychronopoulou K, Costa CN, Cabello Galisteo F, Lopez Granados M, Fierro JLG, Bakas T, Efstathiou AM. Novel Fe-Mn-Ti-O mixed-metal oxides for the low-temperature removal of $H_2S$ from gas streams in the presence of $H_2$, $CO_2$ and $H_2O$. *J Catal*. 2005; 236:205–220.
11. Deshpande PA, Madras G. Noble metal ionic sites for catalytic hydrogen combustion: spectroscopic insights. *Phys Chem Chem Phys*. 2011;13:708–718.
12. Deshpande PA, Madras G. Catalytic hydrogen combustion for treatment of combustible gases from fuel cell processors. *Appl Catal B: Environ*. 2010;100:481–490.
13. Sharma S, Hegde MS. $Ti_{0.99}Pd_{0.01}O_{2-\delta}$: A new Pt-free catalyst for high rates of $H_2+O_2$ recombination with high CO tolerant capacity. *ChemPhysChem*. 2009;10:637–640.
14. Bera P, Hegde MS, Patil KC. Combustion synthesized $Ce_{1-x}Pt_xO_{2-\delta}$ ($x = 0.005$, 0.01, 0.02; $\delta = 0.07$ and 0.1): A novel room-temperature $H_2$-$O_2$ recombination catalyst. *Curr Sci*. 2001;80:1576–1578.
15. Deshpande PA, Madras G. Support dependent activity of noble metal substituted oxide catalysts for the water-gas shift reaction. *AIChE J*. 2010;56:2662–2676.
16. Kalamaras CM, Panagiotopoulou Kondarides DI, Efstathiou AM. Kinetic and mechanistic studies of the water-gas shift reaction on Pt/$TiO_2$ catalyst. *J Catal*. 2009;264:117–129.
17. Kalamaras CM, Americanou S, Efstathiou AM. "Redox" vs "associative formate with –OH group regeneration" WGS mechanism on Pt/$CeO_2$: effect of platinum particle size. *J Catal*. 2011;279:287–300.
18. Kalamaras CM, Olympiou GG, Efstathiou AM. The water-gas shift reaction on Pt/$\gamma$-$Al_2O_3$ catalyst: *operando* SSITKA-DRIFTS-mass spectroscopy studies. *Catal Today*. 2008;138:228–234.
19. Olympiou GG, Kalamaras CM, Zeinalipour-Yazdi CD, Efstathiou AM. Mechanistic aspects of the water-gas shift reaction on alumina-supported noble metal catalysts: in situ DRIFTS and SSITKA-mass spectrometry studies. *Catal Today*. 2007;127:304–318.
20. Trovarelli A. *Catalysis by Ceria and Related Materials*. London: Imperial College Press, 2002.
21. Gorte RJ. Ceria in catalysis: from automotive applications to the water-gas shift reaction. *AIChE J*. 2010;56:1126–1135.
22. Azzam KG, Babich IV, Seshan K, Lefferts L. Bifunctional catalysts for single-stage water-gas shift reaction in fuel cell applications. Part 1. Effect of the support on the reaction sequence. *J Catal*. 2007;251:153–162.
23. Azzam KG, Babich IV, Seshan K, Lefferts L. Bifunctional catalysts for single-stage water-gas shift reaction in fuel cell applications. Part 2. Role of the support and the promoter on catalyst activity and stability. *J Catal*. 2007;251:163–171.
24. Ribeiro MC, Jacobs G, Graham UM, Azzam KG, Linganiso L, Davis BH. Low temperature water-gas shift: differences in the oxidation states observed with partially reduced Pt/$MnO_x$ and Pt/$CeO_x$ catalysts yield differences in OH group activity. *Catal Commun*. 2010;11:1193–1199.
25. Fu Q, Saltsberg H, Flytzani-Stephanopoulos M. Active non-metallic Au and Pt species on ceria—based water-gas shift catalyst. *Science*. 2003;301:935–938.
26. Gayen A, Boaro M, Leitenburg C, Llorca J, Trovarelli A. Activity, durability and microstructural characterization of ex-nitrate and ex-chloride Pt/$Ce_{0.56}Zr_{0.44}O_2$ catalysts for low temperature water-gas shift reaction. *J Catal*. 2010;270:285–298.
27. Barao M, Vicario M, Llorca J, de Leitenberg C, Dolcetti G, Trovarelli A. A comparative study of water-gas shift reaction over gold and platinum supported on $ZrO_2$ and $CeO_2$-$ZrO_2$. *Appl Catal B: Environ*. 2009;88:272–282.
28. Kambolis A, Matralis H, Trovarelli A, Papadopoulou Ch. Ni/$CeO_2$-$ZrO_2$ catalysts for the dry reforming of methane. *Appl Catal A: Gen*. 2010;377:16–26.
29. Yi N, Si R, Saltsburg H, Flytzani-Stephanopoulos M. Active gold species on cerium oxide nanoshapes for methanol steam reforming and the water-gas shift reaction. *Energy Environ Sci*. 2010;3:831–837.
30. Yi N, Si R, Saltsburg H, Flytzani-Stephanopoulos M. Steam reforming of methanol over ceria and gold-ceria nanoshapes. *Appl Catal B: Environ*. 2010;95:87–92.
31. Hegde MS, Madras G, Patil KC. Nobel metal ionic catalysts. *Acc Chem Res*. 2009;42:704–712.
32. Busca G, Leitti L, Ramis G, Berti F. Chemical and mechanistic aspects of the selective catalytic reduction of NO(x) by ammonia over oxide catalysts: a review. *Appl Catal B: Environ*. 1998;18:1–36.
33. Apostolescu N, Geiger B, Hizbullah K, Jan MT, Kureti S, Reichert D, Schott F, Weisweiler W. Selective catalytic reduction of nitrogen oxides by ammonia on iron oxide catalysts. *Appl Catal B: Environ*. 2006;62:104–114.
34. Chaudhary VR, Patil VP, Jena P, Upadhe BS. Nano-gold supported on $Fe_2O_3$: a highly active catalyst for low temperature oxidative destruction of methane green house gas from exhaust/waste gases. *Appl Catal A: Gen*. 2008;350:186–190.
35. Lambrou PS, Efstathiou AM. The effects of Fe on the oxygen storage and release properties of model Pd-Rh/$CeO_2$-$Al_2O_3$ three-way catalyst. *J Catal*. 2006;240:182–193.
36. Lambrou PS, Savva PG, Fierro JLG, Efstathiou AM. The effect of Fe on the catalytic behavior of model Pd-Rh/$CeO_2$-$Al_2O_3$ three way catalysts. *Appl Catal B: Environ*. 2004;76:375–385.
37. Baldychev I, Gorte RJ, Vohs JM. The impact of redox properties on the reactivity of $V_2O_5$/$Al_2O_3$ catalysts. *J Catal*. 2010;269:397–403.
38. Radhika T, Sugunan S. Structural and catalytic investigation of vanadia supported on ceria promoted with high surface area rice husk silica. *J Mol Catal A: Chem*. 2006;250:253–259.
39. Fino D, Russo N, Badini C, Saracco G, Specchia V. Effect of active species mobility on soot-combustion over Cs-V catalysts. *AIChE J*. 2003;49:2173–2180.
40. Taufiq-Yap YH, Waugh KC. A study of the nature of oxidant in $V_2O_5$-$MoO_3$/$Al_2O_3$ catalyst. *Chem Eng Sci*. 2001;56:5787–5792.
41. Pieck CL, del Val S, Granados ML, Banares MA, Fierro JLG. Bulk and surface structures of $V_2O_5$/$ZrO_2$ systems and their revelance for o-xylene oxidation. *Langmuir*. 2002;18:2642–2648.
42. Lewis KB, Oyama ST, Somorjai GA. TPD studies of vanadium oxide films deposited on gold. *Surf Sci*. 1991;52:241–248.
43. Deshpande PA, Madras G. Combustion synthesized vanadia rods for environmental applications. *AIChE J*. Published online; DOI: 10.1002/aic.12418.
44. Patil KC, Hegde MS, Rattan T, Aruna ST. *Chemistry of Nanocrystalline Oxide Materials: Combustion Synthesis, Properties and Applications*. Singapore: World Scientific, 2008.
45. Dixit A, Lawes G. Development of electrical polarization at antiferromagnetic transition in $FeVO_4$. *J Phys: Condens Matter*. 2009;21:456003.
46. Dixit A, Lawes G, Harris AB. Magnetic structure and magnetoelectric coupling in bulk and thin film $FeVO_4$. *Phys Rev B*. 2010;82:024430.
47. Ekambaram S, Patil KC. Rapid synthesis and properties of $FeVO_4$, $AlVO_4$, $YVO_4$ and $Eu^{3+}$-doped $YVO_4$. *J Alloys Compd*. 1995;217: 104–107.
48. Qi G, Yang RT, Rinaldi FC. Selective catalytic reduction of nitric oxide with hydrogen over Pd-based catalysts. *J Catal*. 2006;237: 381–292.
49. Bellakki MB, Baidya T, Shivakumara C, Vasanthacharya NY, Hegde MS, Madras G. Synthesis, characterization, redox and photocatalytic properties of $Ce_{1-x}Pd_xVO_4$ ($0 < \times < 0.1$). *Appl Catal B: Environ*. 2008;84:474–481.
50. Bernal S, Calvino JJ, Cifredo GA, Laachir A, Perrichon V. Influence of the reduction/evacuation conditions on the rate of hydrogen spillover on Rh/$CeO_2$ catalysts. *Langmuir*. 1994;10:717–722.

51. Zafiris GS, Gorte RJ. A study of CO, NO, and $H_2$ adsorption on model Pt/$CeO_2$ catalysts. *Surf Sci*. 1992;276:86–94.
52. Fierro JLG, Soria J, Sanz J, Rojo JM. Induced changes in ceria by thermal treatments under vacuum or hydrogen. *J Solid State Chem*. 1987;66:154–162.
53. Rodriguez LJ, Ruette F, Rosa-Brussin M. Theoretical study of hydrogen activation in a hematite cluster. *J Mol Catal*. 1990;62;199–213.
54. Deshpande PA, Hegde MS, Madras G. A mechaistic model for the water-gas shift reaction over noble-metal substituted ceria. *AIChE J*. 2010;56:1315–1324.

## Appendix A: Derivation of Rate Expression for Dissociative Adsorption Mechanism

The elementary steps for the reaction are

$$H_2 + 2S - CeO \leftrightarrow 2S - H - CeO \tag{15}$$

$$2S - H - CeO + O_L \rightarrow H_2O + S - CeO + S - CeR - v \tag{16}$$

$$S - CeR - v + O_2 \rightarrow S - CeO \cdot O + O_L \tag{17}$$

$$S - CeO \cdot O + H_2 \rightarrow H_2O + S - CeO \tag{18}$$

The rate of reaction is given as

$$r_{H_2} = k_{16}\theta_H^2[O_L] + k_{18}[H_2]\theta_{oo} \tag{A1}$$

where $\theta_H$ and $\theta_\infty$ are the fraction of sites occupied by H and O, respectively.

The equilibrium on Eq. 15 gives

$$k_{15}[H_2]\theta_v^2 = k_{-15}\theta_H^2 \tag{A2}$$

Defining $K_{15} = k_{15}/k_{-15}$

$$\theta_H = \sqrt{K_{15}[H_2]}\theta_v \tag{A2}$$

The site balance for $H_2$ adsorption can be written as

$$\theta_H + \theta_v = 1 \tag{A3}$$

From Eqs. A2 and A3

$$\theta_H = \frac{\sqrt{K_{15}[H_2]}}{1 + \sqrt{K_{15}[H_2]}} \tag{A4}$$

Balance on lattice oxygen [$O_L$]

$$k_{16}\theta_H^2[O_L] = k_{17}\theta_{vo}[O_2] \tag{A5}$$

Balance on oxygen species o

$$k_{17}\theta_{vo}[O_2] = k_{18}\theta_{oo}[H_2] \tag{A6}$$

Balance on $O_2$ adsorption sites

$$\theta_{vo} + \theta_{oo} = 1 \tag{A7}$$

From Eqs. A6 and A7

$$\theta_{oo} = \frac{k_{17}[O_2]}{k_{17}[O_2] + k_{18}[H_2]} \tag{A8}$$

Therefore, from Eqs. A5, A6, and A8, we get the required rate expression as follows

$$r_{H_2} = \frac{2k_{17}k_{18}[H_2][O_2]}{k_{17}[O_2] + k_{18}[H_2]} \tag{A9}$$

## Appendix B: Derivation of Rate Expression for Molecular Adsorption Mechanism

The elementary steps are given as

$$H_2 + S - FeO \leftrightarrow S - H_2 - FeO \tag{21}$$

$$S - H_2 - FeO + O_L \rightarrow H_2O + S - FeR - v \tag{22}$$

$$O_2 + S - FeR - v \rightarrow S - FeO \cdot O + O_L \tag{23}$$

$$H_2 + S - FeO \cdot O \rightarrow H_2O + S - FeO \tag{24}$$

The rate of reaction can be written as

$$r_{H_2} = k_{22}\theta_{H_2}[O_L] + k_{24}\theta_{oo}[H_2] \tag{B1}$$

Equilibrium on Eq. 21 gives

$$k_{21}\theta_v[H_2] = k_{-21}\theta_{H_2} \tag{B2}$$

From Eq. B2 and site balance on $H_2$ adsorption sites

$$\theta_{H_2} = \frac{K_{21}[H_2]}{1 + K_{21}[H_2]} \tag{B3}$$

Balance on lattice oxygen

$$k_{22}\theta_{H_2}[O_L] = k_{23}\theta_{vo}[O_2] \tag{B4}$$

Balance on *o* species

$$k_{23}\theta_{vo}[O_2] = k_{24}\theta_{oo}[H_2] \tag{B5}$$

From Eq. B5 and balance on $O_2$ adsorption sites

$$\theta_{oo} = \frac{k_{23}[O_2]}{k_{23}[O_2] + k_{24}[H_2]} \tag{B6}$$

From Eqs. B4, B5, and B6, the required rate expression

$$r_{H_2} = \frac{2k_{23}k_{24}[H_2][O_2]}{k_{23}[O_2] + k_{24}[H_2]} \tag{B7}$$

## Appendix C: Derivation of Rate Expression for Standard Heterogeneous Catalysis Models (1) Eley Rideal Mechanism

$$O_2 + 2S \leftrightarrow 2O - S \tag{28}$$

$$H_2 + O - S \rightarrow H_2O + S \tag{29}$$

The rate of reaction is given as

$$r_{H_2} = k_{29}[H_2]\theta_o \quad (C1)$$

where $\theta_o$ is the fraction of sites on the catalyst occupied by *O* species. From the equilibrium of Eq. 28 we get

$$k_{28}[O_2]\theta_v^2 = k_{-28}\theta_o^2 \quad (C2)$$

where $\theta_v$ is the fraction of vacant sites on the catalyst. If $K_{28} = \frac{k_{28}}{k_{-28}}$ then

$$\theta_o = \sqrt{K_{28}[O_2]}\theta_v \quad (C3)$$

Site balance on the catalyst gives

$$\theta_o + \theta_v = 1 \quad (C4)$$

From Eqs. C3 and C4

$$\theta_o = \frac{\sqrt{K_{28}[O_2]}}{1 + \sqrt{K_{28}[O_2]}} \quad (C5)$$

Substituting Eq. C5 in C1 we get

$$r_{H_2} = \frac{k_{29}[H_2]\sqrt{K_{28}[O_2]}}{1 + \sqrt{K_{28}[O_2]}} \quad (C6)$$

Equation C6 gives the required rate expression.

**(2) Langmuir-Hinshelwood Mechanism with Dissociative Adsorption of $H_2$**

$$H_2 + 2S \leftrightarrow 2H - S \quad (31)$$

$$O_2 + 2S \leftrightarrow 2O - S \quad (32)$$

$$2H - S + O - S \rightarrow H_2O + 3S \quad (33)$$

The rate of the reaction is given as

$$r_{H_2} = k_{33}\theta_H^2\theta_o \quad (C7)$$

Equilibrium on steps 31 and 32 gives

$$k_{31}[H_2]\theta_v^2 = k_{-31}\theta_H^2 \quad (C8)$$

$$k_{32}[O_2]\theta_v^2 = k_{-32}\theta_o^2 \quad (C9)$$

Defining $K_{31} = \frac{k_{31}}{k_{-31}}$ and $K_{32} = \frac{k_{32}}{k_{-32}}$ we get

$$\theta_H = \sqrt{K_{31}[H_2]}\theta_v \quad (C10)$$

$$\theta_o = \sqrt{K_{32}[O_2]}\theta_v \quad (C11)$$

Balance on sites gives

$$\theta_H + \theta_o + \theta_v = 1 \quad (C12)$$

From Eqs. C10, C11, and C12 we get

$$\theta_H = \frac{\sqrt{K_{31}[H_2]}}{1 + \sqrt{K_{31}[H_2]} + \sqrt{K_{32}[O_2]}} \quad (C13)$$

$$\theta_o = \frac{\sqrt{K_{32}[O_2]}}{1 + \sqrt{K_{31}[H_2]} + \sqrt{K_{32}[O_2]}} \quad (C14)$$

Therefore, substitution of Eqs. C13 and C14 in Eq. C7 gives the required rate expression as

$$r_{H_2} = \frac{k_{33}K_{31}\sqrt{K_{32}}[H_2]\sqrt{[O_2]}}{\left(1 + \sqrt{K_{31}[H_2]} + \sqrt{K_{32}[O_2]}\right)^3} \quad (C15)$$

**(3) Langmuir-Hinshelwood Mechanism with Molecular Adsorption of $H_2$**

$$H_2 + S \leftrightarrow H_2 - S \quad (35)$$

$$O_2 + 2S \leftrightarrow 2O - S \quad (36)$$

$$H_2 - S + O - S \rightarrow H_2O + 2S \quad (37)$$

The rate of reaction is given as

$$r_{H_2} = k_{37}\theta_{H_2}\theta_o \quad (C16)$$

The equilibrium on Eqs. 35 and 36 gives

$$\theta_{H_2} = K_{35}[H_2]\theta_v \quad (C17)$$

$$\theta_o = \sqrt{K_{36}[O_2]}\theta_v \quad (C18)$$

The balance on sites can be written as

$$\theta_{H_2} + \theta_o + \theta_v = 1 \quad (C19)$$

From Eqs. C17, C18, and C19

$$\theta_{H_2} = \frac{K_{35}[H_2]}{1 + K_{35}[H_2] + \sqrt{K_{36}[O_2]}} \quad (C20)$$

$$\theta_o = \frac{\sqrt{K_{36}[O_2]}}{1 + K_{35}[H_2] + \sqrt{K_{36}[O_2]}} \quad (C21)$$

Substitution of Eqs. C20 and C21 in Eq. C16 gives the required rate expression as

$$r_{H_2} = \frac{k_{37}K_{35}[H_2]\sqrt{K_{36}[O_2]}}{\left(1 + K_{35}[H_2] + \sqrt{K_{36}[O_2]}\right)^2} \quad (C22)$$

*Manuscript received Feb. 14, 2011, and revision received Mar. 16, 2011.*